frontiers | Frontiers in Physics

ORIGINAL RESEARCH
published: 11 May 2022
doi: 10.3389/fphy.2022.836784

Ab Initio Wavefunction Analysis of Electron Removal Quasi-Particle State of $NdNiO_2$ With Fully Correlated Quantum Chemical Methods

Vamshi M. Katukuri[1]*, *Nikolay A. Bogdanov*[1] and *Ali Alavi*[1,2]

[1]Max Planck Institute for Solid State Research, Stuttgart, Germany, [2]Yusuf Hamied Department of Chemistry, University of Cambridge, Cambridge, United Kingdom

The discovery of superconductivity in hole-doped infinite-layer $NdNiO_2$ — a transition metal (TM) oxide that is both isostructural and isoelectronic to cuprate superconductors—has lead to renewed enthusiasm in the hope of understanding the origin of unconventional superconductivity. Here, we investigate the electron-removal states in infinite-layered Ni^{1+} oxide, $NdNiO_2$, which mimics hole doping, with the state-of-the-art many-body multireference quantum chemistry methods. From the analysis of the many-body wavefunction we find that the hole-doped d^8 ground state of $NdNiO_2$ is very different from the d^8 ground state in isostructural cuprate analog $CaCuO_2$, although the parent d^9 ground states are for the most part identical. We show that the doped hole in $NdNiO_2$ mainly localizes on the Ni $3d_{x^2-y^2}$ orbital to form a closed-shell singlet, and this singlet configuration contributes to ~40% of the wavefunction. In contrast, in $CaCuO_2$ the Zhang-Rice singlet configurations contribute to ~65% of the wavefunction. With the help of the quantum information concept of entanglement entropy, we quantify the different types of electronic correlations in the nickelate and cuprate compounds, and find that the dynamic radial-type correlations within the Ni *d* manifold are persistent in hole-doped $NdNiO_2$. As a result, the d^8 multiplet effects are stronger and the additional hole foot-print is more three-dimensional in $NdNiO_2$. Our analysis shows that the most commonly used three-band Hubbard model employed to express the doped scenario in cuprates represents ~90% of the d^8 wavefunction for $CaCuO_2$, but such a model grossly approximates the d^8 wavefunction for $NdNiO_2$ as it only stands for ~60% of the wavefunction.

Keywords: nickelates, superconductors, wavefunction quantum chemistry, doped-holes, ab initio

OPEN ACCESS

Edited by:
Danfeng Li,
City University of Hong Kong, Hong Kong SAR, China

Reviewed by:
Frank Lechermann,
European X-Ray Free Electron Laser, Germany
BaiYang Wang,
Stanford University, United States

****Correspondence:***
Vamshi M. Katukuri
V.Katukuri@fkf.mpg.de

Specialty section:
This article was submitted to Condensed Matter Physics, a section of the journal Frontiers in Physics

Received: *15 December 2021*
Accepted: *14 March 2022*
Published: *11 May 2022*

Citation:
Katukuri VM, Bogdanov NA and Alavi A (2022) Ab Initio Wavefunction Analysis of Electron Removal Quasi-Particle State of $NdNiO_2$ With Fully Correlated Quantum Chemical Methods. Front. Phys. 10:836784. doi: 10.3389/fphy.2022.836784

1 INTRODUCTION

For more than 3 decades, understanding the mechanism of superconductivity observed at high critical temperature (HTC) in strongly correlated cuprates [1] has been the "holy grail" of many theoretical and experimental condensend matter researchers. In this context, the observation of superconductivity in nickelates $LnNiO_2$, *Ln* = {La, Nd and Pr} [2–4] upon doping with holes is

remarkable. These superconducting nickelates are isostructural as well as isoelectronic to HTC cuprate superconductors and thus enable the comparison of the essential physical features that may be playing a crucial role in the mechanism driving superconductivity.

LnNiO_2 family of compounds are synthesized in the so-called infinite-layer structure, where NiO_2 and *Ln* layers are stacked alternatively [2]. The NiO_2 planes are identical to the CuO_2 planes in HTC cuprates which host much of the physics leading to superconductivity [5]. A simple valence counting of the these nickelates reveals a 1+ oxidation state for Ni (2- for O and 3+ for *Ln*) with nine electrons in the 3*d* manifold. In the cuprates, the Cu^{2+} oxidation state gives rise to the same $3d^9$ electronic configuration. Contrary to many nickel oxides where the Ni atom sits in an octahedral cage of oxygens, in the infinite-layered structure, square planar NiO_4 plaques are formed without the apical oxygens. The crystal field due to square-planar oxygen coordination stabilizes the d_{z^2} orbital of the e_g manifold, making its energy close to the t_{2g} orbitals (the 3*d* orbitals split to 3-fold t_{2g} and 2-fold e_g sub-shells in an octahedral environment). With d^9 occupation, a half-filled $d_{x^2-y^2}$-orbital system is realized as in cuprates. In fact, recent resonant inelastic X-ray scattering (RIXS) experiments [6] as well as the *ab initio* correlated multiplet calculations [7] confirm that the Ni^{1+} *d-d* excitations in $NdNiO_2$ are similar to the Cu^{2+} ions in cuprates [8].

Several electronic structure calculations based on density-functional theory (DFT) have shown that in monovalent nickelates the Ni $3d_{x^2-y^2}$ states sit at the Fermi energy level [9–11]. These calculations further show that the nickelates are more close to the Mott-Hubbard insulating limit with a decreased Ni *3d*- O *2p* hybridization compared to cuprates. The latter are considered to be charge transfer insulators [12] where excitations across the electronic band gap involves O 2*p* to Cu 3*d* electron transfer. Correlated wavefunction-based calculations [7] indeed find that the contribution from the O 2*p* hole configuration to the ground state wavefunction in $NdNiO_2$ is four times smaller than in the cuprate analogue $CaCuO_2$. X-ray absorption and photoemission spectroscopy experiments [13, 14] confirm the Mott behavior of nickelates.

In the cuprate charge-transfer insulators, the strong hybridization of the Cu $3d_{x^2-y^2}$ and O 2*p* orbitals result in O 2*p* dominated bonding and Cu $3d_{x^2-y^2}$ -like antibonding orbitals. As a consequence, the doped holes primarily reside on the bonding O 2*p* orbitals, making them singly occupied. The unpaired electrons on the Cu $d_{x^2-y^2}$ and the O 2*p* are coupled antiferromagnetically resulting in the famous Zhang-Rice (ZR) spin singlet state [15]. In the monovalent nickelates, it is unclear where the doped-holes reside. Do they form a ZR singlet as in cuprates? Instead, if the holes reside on the Ni site, do they form a high-spin local triplet with two singly occupied Ni 3*d* orbitals and aligned ferromagnetically or a low-spin singlet with either both the holes residing in the Ni $3d_{x^2-y^2}$ orbital or two singly occupied Ni 3d orbitals but aligned anti-parallel. While Ni L-edge XAS and RIXS measurements [6] conclude that an orbitally polarized singlet state is predominant, where doped holes reside on the Ni $3d_{x^2-y^2}$ orbital, O K-edge electron energy loss spectroscopy [14] reveal that some of the holes also reside on the O 2*p* orbitals. On the other hand, calculations based on multi-band $d-p$ Hubbard models show that the fate of the doped holes is determined by a subtle interplay of Ni onsite (U_{dd}), Ni *d* - O 2*p* inter-site (U_{dp}) Coulomb interactions and the Hund's coupling along with the charge-transfer gap [16, 17]. However, with the lack of extensive experimental data, it is difficult to identify the appropriate interaction parameters for a model Hamiltonian study, let alone identifying the model that best describes the physics of superconducting nickelates.

Despite the efforts to discern the similarities and differences between the monovalent nickelates and superconducting cuprates, there is no clear understanding on the nature of doped holes in $NdNiO_2$. Particularly, there is no reliable parameter-free *ab initio* analysis of the hole-doped situation. In this work, we investigate the hole-doped ground state in $NdNiO_2$ and draw parallels to the hole-doped ground state of cuprate analogue $CaCuO_2$. We use fully *ab initio* many-body wavefunction-based quantum chemistry methodology to compute the ground state wavefunctions for the hole-doped $NdNiO_2$ and $CaCuO_2$. We find that the doped hole in $NdNiO_2$ mainly localizes on the Ni $3d_{x^2-y^2}$ orbital to form a closed-shell singlet, and this singlet configuration contributes to ~40% of the wavefunction. In contrast, in $CaCuO_2$ the Zhang-Rice singlet configurations contribute to ~65% of the wavefunction. The persistent dynamic radial-type correlations within the Ni *d* manifold result in stronger d^8 multiplet effects than in $CaCuO_2$, and consequently the additional hole foot-print is more three-dimensional in $NdNiO_2$. Our analysis shows that the most commonly used three-band Hubbard model to express the doped scenario in cuprates represents 90% of the d^8 wavefunction for $CaCuO_2$, but such a model grossly approximates the d^8 wavefunction for the $NdNiO_2$ as it only stands for ~60% of the wavefunction.

In what follows, we first describe the computational methodology we use in this work where we highlight the novel features of the methods and provide all the computational details. We then present the results of our calculations and conclude with a discussion.

2 THE WAVEFUNCTION QUANTUM CHEMISTRY METHOD

Ab initio configuration interaction (CI) wavefunction-based quantum chemistry methods, particularly the post Hartree-Fock (HF) complete active space self-consistent field (CASSCF) and the multireference perturbation theory (MRPT), are employed. These methods not only facilitate systematic inclusion of electron correlations, but also enable to quantify different types of correlations, static vs. dynamic [18]. These calculations do not use any *ad hoc* parameters to incorporate electron-electron interactions unlike other many-body methods, instead, they are computed fully *ab initio* from the kinetic and Coulomb integrals. Such *ab initio* calculations provide techniques to systematically analyze electron correlation effects and offer insights into the electronic structure of correlated solids that go substantially beyond standard DFT approaches,

e.g., see Refs. [7, 19–22] for the 3*d* TM oxides and Refs. [23–27] for 5*d* compounds.

2.1 Embedded Cluster Approach

Since strong electronic correlations are short-ranged in nature [28], a local approach for the calculation of the N and $N \pm 1$ –electron wavefunction is a very attractive option for transition metal compounds. In the embedded cluster approach, a finite set of atoms, we call quantum cluster (QC), is cut out from the infinite solid and many-body quantum chemistry methods are used to calculate the electronic structure of the atoms within the QC. The cluster is "embedded" in a potential that accounts for the part of the crystal that is not treated explicitly. In this work, we represent the embedding potential with an array of point charges (PCs) at the lattice positions that are fitted to reproduce the Madelung crystal field in the cluster region [29]. Such procedure enables the use of quantum chemistry calculations for solids involving transition-metal or lanthanide ions, see Refs. [23, 30, 31].

2.2 Complete Active Space Self-Consistent Field

CASSCF method [18] is a specific type of multi-configurational (MC) self-consistent field technique in which a complete set of Slater determinants or configuration state functions (CSFs) that is used in the expansion of the CI wavefunction is defined in a constrained orbital space, called the active space. In the CASSCF(n,m) approach, a subset of n active electrons are fully correlated among an active set of m orbitals, leading to a highly multi-configurational (CAS) reference wavefunction. CASSCF method with a properly chosen active space guarantees a qualitatively correct wavefunction for strongly correlated systems where static correlation [18] effects are taken into account.

We consider active spaces as large as CAS(24,30) in this work. Because the conventional CASSCF implementations based on deterministic CI space (the Hilbert space of all possible configurations within the active space) solvers are limited to active spaces of 18 active electrons in 18 orbitals, we use the full configuration interaction quantum Monte Carlo (FCIQMC) [32–34] and density matrix renormalization group (DMRG) theory [35, 36] algorithms to solve the eigenvalue problem defined within the active space.

2.3 Multireference Perturbation Theory

While the CASSCF calculation provides a qualitatively correct wavefunction, for a quantitative description of a strongly correlated system, dynamic correlations [18] (contributions to the wavefunction from those configurations related to excitations from inactive to active and virtual, and active to virtual orbitals) are also important and must be accounted for. A natural choice is variational multireference CI (MRCI) approach where the CI wavefunction is extended with excitations involving orbitals that are doubly occupied and empty in the reference CASSCF wavefunction [18]. An alternative and computationally less demanding approach to take into account the dynamic correlations is based on perturbation theory in second- and higher-orders. In multireference perturbation theory (MRPT) MC zeroth-order wavefunction is employed and excitations to the virtual space are accounted by means of perturbation theory. If the initial choice of the MC wavefunction is good enough to capture the large part of the correlation energy, then the perturbation corrections are typically small. The most common variations of MRPT are the complete active space second-order perturbation theory (CASPT2) [37] and the n-electron valence second-order perturbation theory (NEVPT2) [38] which differ in the type of zeroth-order Hamiltonian H_0 employed.

TABLE 1 | The different active spaces (CAS) considered in this work. NEL is number of active electrons and NORB is the number of active orbitals. The numbers in parenthesis indicate the orbital numbers in **Figure 2**.

CAS	NEL	NORB
CAS-1	18	24 (1–24)
CAS-2	24	30 (1–30)
CAS-3[a]	12	14 (1, 6, 11, 16 and 21–30)

[a]*The four neighbouring Ni^{1+} (Cu^{2+}) ions in the quantum cluster are treated as closed shell Cu^{1+} (Zn^{2+}) ions.*

3 THE *AB INITIO* MODEL

Before we describe the *ab initio* model we consider, let us summarize the widely used and prominent model Hamiltonian to study the nature of doped hole in HTC cuprates and also employed for monovalent nickelates lately. It is the three-band Hubbard model [39] with three orbital degrees of freedom (bands) which include the d orbital of Cu with x^2-y^2 symmetry and the in-plane oxygen p orbitals aligned in the direction of the nearest Cu neighbours. These belong to the b_1 irreducible representation (irrep) of the D_{4h} point group symmetry realized at the Cu site of the CuO_4 plaque, the other Cu d orbitals belong to a_1 (d_{z^2}), b_2 (d_{xy}) and e ($d_{xz,yz}$) irreps. The parameters in this Hamiltonian include the most relevant hopping and Coulomb interactions within this set of orbitals. More recently, the role of the Cu 3*d* multiplet structure on the hole-doped ground state is also studied [40]. While this model explains certain experimental observations, there is still a huge debate on what is the minimum model to describe the low-energy physics of doped cuprates. Nevertheless, this model has also been employed to investigate the character of the doped hole in monovalent nickelates [16, 17, 41].

Within the embedded cluster approach described earlier, we consider a QC of five NiO_4 (CuO_4) plaques that includes five Ni (Cu) atoms, 16 oxygens and 8 Nd (Ca) atoms, see **Figure 1**. The 10 Ni (Cu) ions neighbouring to the cluster are also included in the QC, however, these are considered as total ion potentials (TIPs). The QC is embedded in point charges that reproduce the electrostatic field of the solid environment. We used the crystal structure parameters for the thin film samples reported in Refs. [2, 42–44].

We used effective core potentials [45] and correlation consistent basis sets of triple-ζ quality with additional

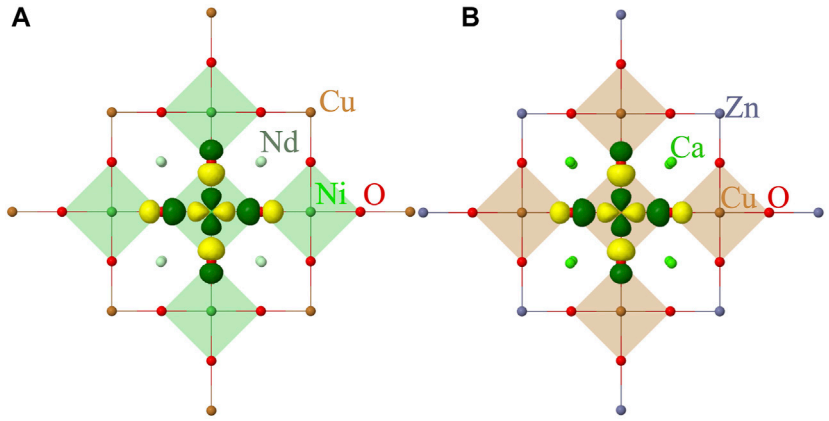

FIGURE 1 | Quantum cluster of five NiO_4 **(A)** and CuO_4 **(B)** plaques considered in our calculations. The point-charge embedding is not shown. The symmetry adapted localized $3d_{x^2-y^2}$ and the oxygen Zhang-Rice-like $2p$ orbitals, the basis in which the wavefunction in **Table 3** is presented are shown in yellow and green color.

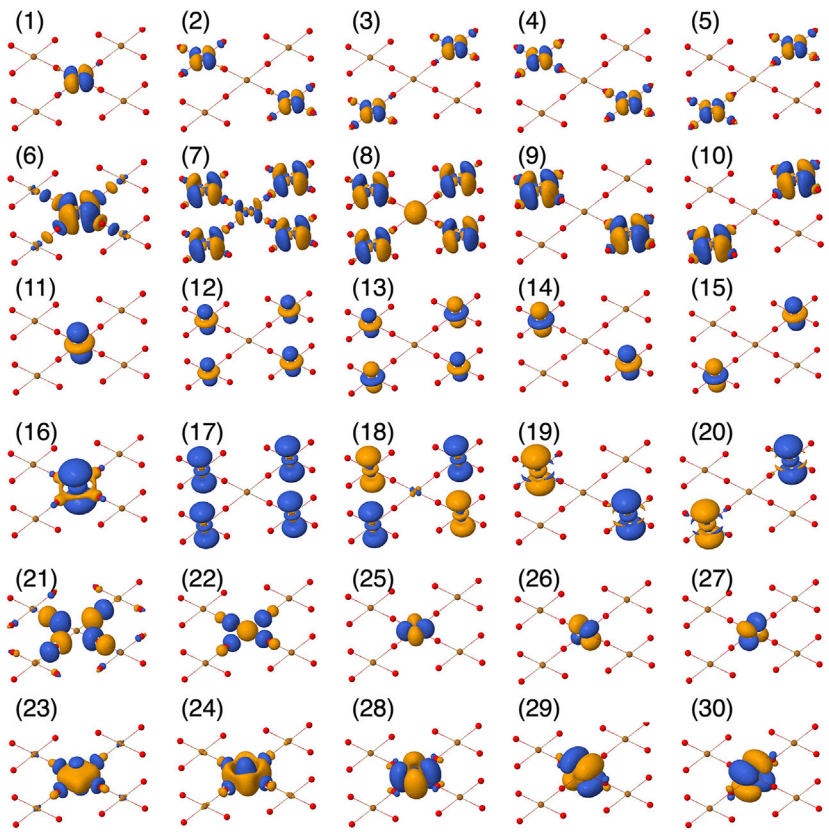

FIGURE 2 | Active orbital basis used in the CASSCF calculations, plotted using Jmol [54].

polarization functions—[$4s3p3d1f$]—for Ni (Cu) [46] and double-ζ quality—[$3s2p1d$]—for oxygens [47]. For the eight Nd (Ca) atoms large core effective potentials [48–50] and associated [$3s2p2d$] basis functions were used. In the case of Nd, the f-electrons were incorporated in the core. Cu^{1+} (Zn^{2+}) total ion potentials (TIPs) with [$2s1p$] functions were used for the 10 Ni^{1+} (Cu^{2+}) [51, 52] peripheral ions of the QC.

To investigate the role of different interactions in the d^8 ground state, two different active spaces were considered. In the first active space, CAS-1 in **Table 1**, only the orbitals in the b_1 and a_1 irreps are active. These are $d_{x^2-y^2}$ and d_{z^2}-like orbitals respectively, and the corresponding double-shell $4d$ orbitals of each of the five Ni (Cu) atoms. CAS-1 also contains the symmetry-adapted ZR-like composite O $2p$ and the double-

TABLE 2 | Relative energies (in eV) of the electron removal d^8 states in $NdNiO_2$ and the iso-structural $CaCuO_2$ obtained from CAS(12,14)SCF and CASSCF + CASPT2 calculations.

State	$NdNiO_2$		$CaCuO_2$	
	CASSCF	+CASPT2	CASSCF	+CASPT2
$^1A_{1g}$	0.00	0.00	0.00	0.00
$^3B_{1g}$	1.35	1.88	2.26	2.50
$^1B_{1g}$	2.98	3.24	3.21	3.33

shell 3*p*-like orbitals, numbers 1–20 and 21–24 in **Figure 2**. At the mean-field HF level of theory, there are 16 electrons within this set of orbitals, resulting in CAS(16,22) active space. In the second active space, CAS-2, orbitals of b_2 and the *e* irreps from the central Ni (Cu) *d* manifold are also included. These are the $3d_{xy}$, $3d_{xz,yz}$-like orbitals and the corresponding 4*d* orbitals and the six electrons, numbers 25–30 in **Figure 2**, resulting in a CAS(24,30) active space. The latter active space takes into account the d^8 multiplet effects within the 3*d* manifold explicitly.

The two active spaces considered in this work not only describe all the physical effects included in the above mentioned three-band Hubbard model but go beyond. More importantly, we do not have any *ad-hoc* input parameters for the calculation as all the physical interactions are implicitly included in the *ab initio* Hamiltonian describing the actual scenario in the real materials. We employed OPENMOLCAS [53] quantum chemistry package for all the calculations.

4 RESULTS

4.1 Ground State of the d^8 Configuration

Starting from the electronic structure of the parent compounds, where each Ni (Cu) is in the d^9 configuration, we compute the electron-removal (in the photoemission terminology) d^8 state to investigate the hole-doped quasiparticle state. Since the parent compounds in d^9 configuration have strong nearest neighbour antiferromagnetic (AF) correlations [7], the total spin of our QC in undoped case, with five Ni (Cu) sites, in the AF ground state is S_{QC} = 3/2. By introducing an additional hole (or removing an electron) from the central Ni (Cu) in our QC, the S_{QC} values range from 0 to 3. To simplify the analysis of the distribution of the additional hole, we keep the spins on the four neighbouring Ni (Cu) sites parallelly aligned in all our calculations and from now on we only specify the spin multiplicity of the central Ni (Cu)O_4 plaque. The multiplet structure of the d^8 configuration thus consists of only spin singlet and triplet states, spanned by the four irreps of the 3*d* manifold. The active spaces we consider in this work allow us to compute accurately the excitations only within the b_1 and a_1 irreps [55] and we address the full multiplet structure elsewhere.

When computing the local excitations, a local singlet state on the central Ni (Cu) corresponds to a total spin on the cluster S_{QC} = 2. However, a local triplet state, with central spin aligned parallel to the neighboring spins, corresponds to S_{QC} = 3 and do not satisfy the AF correlations. To avoid the spin coupling between the central d^8 Ni (Cu) with the neighbouring d^9 Ni (Cu) ions, we replace the latter with closed shell, Cu (Zn) d^{10}, ions and freeze them at the mean-field HF level. Such a simplification is justified, as the local excitation energy we compute is an order of magnitude larger than the exchange interaction [7].

In **Table 2**, the relative energies of the lowest local spin singlets $^1A_{1g}$, $^1B_{1g}$ and spin triplet $^3B_{1g}$ states are shown. These are obtained from CASSCF + CASPT2 calculations with CAS(12,14) active space (CAS-3 in **Table 1**) which includes the 3*d* and 4*d* orbitals of the central Ni (Cu) ion and the in-plane O 2*p* and 3*p* orbitals in the b_1 irrep. In the CASPT2 calculation, the remaining doubly occupied O 2*p*, the central Ni (Cu) 3*s* and 3*p* orbitals and all the unoccupied virtual orbitals are correlated.

It can be seen that the ground state is of $^1A_{1g}$ symmetry and the lowest triplet excited state, with $^3B_{1g}$ symmetry, is around 1.88 and 2.5 eV for $NdNiO_2$ and $CaCuO_2$ respectively. The AF magnetic exchange in these two compounds is 76 and 208 meV respectively [7], and thus we expect that our simplification of making the neighbouring d^9 ions closed shell do not over/underestimate the excitation energies. At the CASSCF level, the $^1A_{1g}$-$^3B_{1g}$ excitation energy is 1.35 eV in $NdNiO_2$ while it is 2.26 eV in $CaCuO_2$. Interestingly, the inclusion of dynamical correlations via the CASPT2 calculation, the $^1A_{1g}$ in $NdNiO_2$ is stabilized by 0.53 eV compared to $^3B_{1g}$ state. However, in $CaCuO_2$, the $^1A_{1g}$ state is stabilized by only 0.24 eV. This indicates that the dynamical correlations are more active in the $^1A_{1g}$ state in $NdNiO_2$ than in $CaCuO_2$. We note that the hole excitations within the 3*d* orbitals in the irreps b_2 and *e*, calculated with this limited active space (CAS-3) results in energies lower than the $^3B_{1g}$ and $^1B_{1g}$ states. However, an accurate description of those states requires an enlarged active space that includes not only the same symmetry oxygen 2*p* and 3*p* orbitals from the central NiO_4 plaque but also the 3*d*, 4*d* manifold of the neighbouring Ni (Cu) ions, making the active space prohibitively large. Here, we concentrate on the analysis of the $^1A_{1g}$ ground state and address the complete d^8 multiplet spectrum elsewhere.

4.2 Wavefunction of the d^8 Ground State

The $^1A_{1g}$ ground wavefunction in terms of the weights of the four leading Slater determinants (SD) (in the case of $CaCuO_2$) is

TABLE 3 | Ni and Cu $3d^8$ $^1A_{1g}$ ground state wavefunction: Weights (%) of the leading configurations in the wavefunction computed for $NdNiO_2$ and $CaCuO_2$ with active spaces CAS-1 and CAS-2 (see **Table 1**). d_{b_1} and p_{b_1} are the localized Ni (Cu) $3d_{x^2-y^2}$ and the oxygen 2*p* ZR-like orbitals (see **Figure 1**) in the b_1 irrep respectively. Arrows in the superscript indicate the spin of the electrons and a □ indicates two holes.

	$NdNiO_2$		$CaCuO_2$	
$^1A_{1g}$	CAS-1	CAS-2	CAS-1	CAS-2
$\|d^{\square}_{b_1} p^{\uparrow\downarrow}_{b_1}\rangle$	51.87	42.40	4.20	20.25
$\|d^{\uparrow}_{b_1} p^{\downarrow}_{b_1}\rangle$	8.27	10.48	42.58	38.52
$\|d^{\downarrow}_{b_1} p^{\uparrow}_{b_1}\rangle$	6.07	7.60	25.00	25.60
$\|d^{\uparrow\downarrow}_{b_1} p^{\square}_{b_1}\rangle$	0.09	0.23	21.56	5.14

TABLE 4 | Dominant ten Slater derterminants and their weights (in %) in the d^8 wavefunction for $NdNiO_2$ (we also show the 11th which is the same as the fourth configuration in **Table 3**). The wavefunction is represented in the same basis as the wavefunction in **Table 3**. However, for convenience we use the orbital numbers from **Figure 2** in the first row to express the basis. These orbitals are visually very close to the actual basis. The doubly occupied orbitals are shown as ↑↓, the singly occupied ones with ↑(↓) for spin $\frac{1}{2}$ ($\frac{-1}{2}$) and an empty box implies that the orbital is unoccupied. The red (electrons removed) and green (electrons added) colors indicate the orbitals involved in the excitation starting from the first configuration. The red box indicates that the orbital becomes empty in this particular excited configuration.

	1	2	3	4	5	6	7	8	9	10	11	12	13	14	15	16	17	18	19	20	21	22	23	24	25	26	27	28	29	30	Wt. (%)
1		↓	↓	↓	↓						↑↓	↑↓	↑↓	↑↓	↑↓						↑↓	↑↓			↑↓	↑↓	↑↓				42.40
2	↓	↓	↓	↓	↓						↑↓	↑↓	↑↓	↑↓	↑↓						↑	↑↓			↑↓	↑↓	↑↓				10.48
3	↑	↓	↓	↓	↓						↑↓	↑↓	↑↓	↑↓	↑↓						↓	↑↓			↑↓	↑↓	↑↓				7.6
4	↓	□	↓	↓	↓						↑↓	↑↓	↑↓	↑↓	↑↓						↑↓	↑↓			↑↓	↑↓	↑↓				2.45
5	↓	↓	□	↓	↓						↑↓	↑↓	↑↓	↑↓	↑↓						↑↓	↑↓			↑↓	↑↓	↑↓				2.38
6	↑↓	↓	↓	↓	↓						□	↑↓	↑↓	↑↓	↑↓						↑↓	↑↓			↑↓	↑↓	↑↓				0.61
7		↓	↓	↓	↓						↑↓	□	↑↓	↑↓	↑↓		↑↓				↑↓	↑↓			↑↓	↑↓	↑↓				0.6
8		↓	↓	↓	↓						↑↓	↑↓	□	↑↓	↑↓			↑↓			↑↓	↑↓			↑↓	↑↓	↑↓				0.6
9	↑↓	↓	↓	↓	↓						↑↓	↑↓	↑↓	↑↓	↑↓						↑↓	↑↓			↑↓	□	↑↓				0.48
10	↑↓	↓	↓	↓	↓						↑↓	↑↓	↑↓	↑↓	↑↓						↑↓	↑↓			↑↓	↑↓	□				0.48
11	↑↓	↓	↓	↓	↓						↑↓	↑↓	↑↓	↑↓	↑↓						□	↑↓			↑↓	↑↓	↑↓				0.23

shown in **Table 3**. The wavefunctions corresponding to the CASSCF calculations with the active spaces CAS-1 and CAS-2 are shown. The basis in which the wavefunctions are represented is constructed in two steps: 1) A set of natural orbitals are generated by diagonalising the CASSCF one-body reduced density matrix. 2) To obtain a set of atomic-like symmetry-adapted localized orbital basis, we localize the Ni (Cu) $3d$ and O $2p$ orbitals on the central NiO_4 (CuO_4) plaque through a unitary transformation. Such partial localization within the active space keeps the total energy unchanged. The resulting $3d_{x^2-y^2}$ and the ZR-like oxygen $2p$ orbital basis is shown in **Figure 1**. FCIQMC calculation was performed in this partial localized basis to obtain the wavefunction as a linear combination of SDs. 10 million walkers were used to converge the FCIQMC energy to within 0.1 mHartree.

From **Table 3** it can be seen that the electron-removal d^8 ground state wavefunction for the two compounds is mostly described by the four configurations spanned by the localized $3d_{x^2-y^2}$ (d_{b_1}) and the symmetry-adapted ZR-like oxygen $2p$ (p_{b_1}) orbitals that are shown in **Figure 1**. Let us first discus the wavefunction obtain from the CAS-1 active space. For $NdNiO_2$, the dominant configuration involves two holes on $3d_{x^2-y^2}$, $|d^{\square}_{b_1} p^{\uparrow\downarrow}_{b_1}\rangle$, and contributes to ~52% of the wavefunction, while the configurations that make up the ZR singlet, $|d^{\uparrow}_{b_1} p^{\downarrow}_{b_1}\rangle$ and $|d^{\downarrow}_{b_1} p^{\uparrow}_{b_1}\rangle$, contributes to only ~14%. On the other hand, the d^8 $^1A_{1g}$ state in $CaCuO_2$ is predominantly the ZR singlet with ~68% weight. In the CASSCF calculation with CAS-2 active space, where all the electrons in the $3d$ manifold are explicitly correlated, we find that the character of the wavefunction remains unchanged in $NdNiO_2$ but weight on the dominant configurations is slightly reduced. On the other hand, in $CaCuO_2$, while the contribution from the ZR singlet is slightly reduced, the contribution from $|d^{\square}_{b_1} p^{\uparrow\downarrow}_{b_1}\rangle$ configuration is dramatically increased at the expense of the weight on $|d^{\uparrow\downarrow}_{b_1} p^{\square}_{b_1}\rangle$. This demonstrates that the additional freedom provided by the d_{xy} and $d_{xz/yz}$ orbitals for the electron correlation helps to accommodate the additional hole on the Cu ion.

We note that the four configurations shown in **Table 3** encompass almost 90% of the d^8 wavefunction (with CAS-2 active space) in $CaCuO_2$. Thus, the use of a three-band Hubbard model [39, 40] to investigate the role of doped holes in CuO_2 planes is a reasonable choice. However, for $NdNiO_2$ these configurations cover only 60% of the d^8 wavefunction, hence a three-band Hubbard model is too simple to describe the hole-doped monovalent nickelates.

In **Table 4** and **Table 5**, we show the first ten dominant SD configurations by weight in the d^8 wavefunction of $NdNiO_2$ and $CaCuO_2$ respectively. Interestingly, the configurations with two holes in the out-of-plane d-orbitals d_{z^2} (configuration 6) and $d_{xz/yz}$ (9 and 10 configurations) is significant in $NdNiO_2$, while such configurations do not exist in the dominant ten for $CaCuO_2$. We also find the additional hole to be more delocalized on to the neighboring Ni ions in $NdNiO_2$ than it is in $CaCuO_2$, however, this observation should be taken with precaution as the oxygen environment around the neighboring Ni/Cu ions is only described at the mean-field level in our calculation setup.

A more intuitive and visual understanding of the distribution of the additional hole can be obtained by plotting the difference of the d^8 and the d^9 ground state electron densities as shown in **Figure 3**. Electron density of a multi-configurational state can be computed as a sum of densities arising from the natural orbitals and corresponding (well-defined) occupation numbers. We used Multiwfn program [56] to perform this summation. The negative values of the heat map of the electron density difference (blue color) and the positive values (in red) represent respectively the extra hole density and additional electron density in d^8 state compared to the d^9 state. From **Figure 3A**/**Figure 3C** that show the density difference in the NiO_2/CuO_2 planes (xy-plane), we conclude the following:

1. The hole density is concentrated on the Ni site (darker blue) with b_1 ($d_{x^2-y^2}$) symmetry in $NdNiO_2$ whereas it is distributed evenly on the four oxygen and the central Cu ions with b_1 symmetry in $CaCuO_2$, a result consistent with the wavefunction reported in **Table 3**.

TABLE 5 | Dominant ten SD configurations and their weights (in %) in the d^8 wavefunction for $CaCuO_2$. See the caption of **Table 4** for details of the wavefunction representation.

	1	2	3	4	5	6	7	8	9	10	11	12	13	14	15	16	17	18	19	20	21	22	23	24	25	26	27	28	29	30	Wt
1	↓	↓	↓	↓	↓						↑↓	↑↓	↑↓	↑↓	↑↓						↑	↑↓			↑↓	↑↓	↑↓				38.52
2	↑	↓	↓	↓	↓						↑↓	↑↓	↑↓	↑↓	↑↓						↓	↑↓			↑↓	↑↓	↑↓				25.60
3	□	↓	↓	↓	↓						↑↓	↑↓	↑↓	↑↓	↑↓						↑↓	↑↓			↑↓	↑↓	↑↓				20.25
4	↑↓	↓	↓	↓	↓						↑↓	↑↓	↑↓	↑↓	↑↓						□	↑↓			↑↓	↑↓	↑↓				5.14
5	↓	□	↓	↓	↓						↑↓	↑↓	↑↓	↑↓	↑↓						↑↓	↑↓			↑↓	↑↓	↑↓				1.30
6	↓	↓	□	↓	↓						↑↓	↑↓	↑↓	↑↓	↑↓						↑↓	↑↓			↑↓	↑↓	↑↓				1.27
7	↓	↑↓	↓	↓	↓						↑↓	↑↓	↑↓	↑↓	↑↓						□	↑↓			↑↓	↑↓	↑↓				0.24
8	↓	↓	↑↓	↓	↓						↑↓	↑↓	↑↓	↑↓	↑↓						□	↑↓			↑↓	↑↓	↑↓				0.23
9	↑↓	↓	↓	↓	↓						↓	↑↓	↑↓	↑↓	↑↓	↑					□	↑↓			↑↓	↑↓	↑↓				0.13
10	↑↓	↓	↓	↓	↓						↑	↑↓	↑↓	↑↓	↑↓	↓					□	↑↓			↑↓	↑↓	↑↓				0.12

2. In $NdNiO_2$, the hole density is spread out around the Ni ion with larger radius, and otherwise in $CaCuO_2$. This demonstrates that the 3*d* manifold in Cu is much more localized than in Ni and therefore the onsite Coulomb repulsion *U* is comparatively smaller for Ni.
3. The darker red regions around the Ni site in $NdNiO_2$ indicate stronger d^8 multiplet effects that result in rearrangement of electron density compared to d^9 configuration.
4. In $CaCuO_2$, we see darker red regions on the oxygen ions instead, which shows that the significant presence of a hole on these ions results in noticeable electron redistribution.

The electron density difference in the xz-plane (which is perpendicular to the NiO_2/CuO_2 planes) is quite different in the two compounds. The hole density in $NdNiO_2$ is spread out up to 2 Å in the *z*-direction, unlike in $CaCuO_2$, where it is confined to within 1 Å. We attribute this to the strong radial-type correlations in $NdNiO_2$. With the creation of additional hole on the $3d_{x^2-y^2}$ orbital, the electron density which is spread out in the d_{z^2} symmetry via the dynamical correlation between $3d_{z^2}$ and $4d_{z^2}$ orbitals [7], becomes more compact in the d_{z^2} symmetry through the reverse breathing. Thus, we see a strong red region with $3d_{z^2}$ profile and a blue region with expanded $4d_{z^2}$ profile.

To obtain a quantitative understanding of the charge density differences for the two compounds, in **Figure 3E** we plot the electron density difference integrated over a sphere centered on the central Ni(Cu) atom as a function of the radius *r* shown in **Figure 3A**. Four features, which we marked A-D, clearly demonstrate the contrast in the charge density differences in the two compounds. From the feature A at *r* close to Ni (Cu), it is evident that the extent of hole density around Ni in $NdNiO_2$ is larger than around Cu in $CaCuO_2$. The features B and C that are on either side of the position of oxygen ions show that the hole density is significantly larger on oxygen atoms in $CaCuO_2$ than in $NdNiO_2$. It is interesting to note that we see a jump (feature D) in the electron density above zero at *r* close to the position of Nd ions in $NdNiO_2$, while in $CaCuO_2$ the curve is flat in the region of Ca ions. This shows that there is some electron redistribution happening around the Nd ions. The hole density within a solid sphere (SS) around the central Ni (Cu) atom obtained by additional integration over the radius *r* is also shown in **Figure 3E** with dashed curves. It can be seen that the total hole density within the SS of *r* ~4 Å, where the neighboring Ni (Cu) ions are located, is only ~0.5 in both the compounds, with slight differences related to the feature D. This is due to the screening of the hole with the electron density pulled in from the farther surroundings. As one would expect, a SS with *r* of the size of the cluster, the total hole density is one in both the compounds.

4.3 Orbital Entanglement Entropy

To analyse the different type of correlations active in the two compounds in d^8 configuration, we compute the entanglement entropy [57–59]. While the single orbital entropy, $s(1)_i$, quantifies the correlation between *i*th orbital and the remaining set of orbitals, the mutual information, $I_{i,j}$ is the two-orbital entropy between *i* and *j* [60, 61], and illustrates the correlation of an orbital with another, in the embedded environment comprising of all other orbitals. We used QCMAQUIS [63] embedded in OPENMOLCAS [54] package to compute the entropies.

In **Figure 4**, $s(1)_i$ and $I_{i,j}$ extracted from the d^8 ground state CASSCF calculations with CAS-2 active space for $NdNiO_2$ and $CaCuO_2$ are shown. The orbital basis for which the entropy is computed is the same as the basis in which the wavefunction presented in **Table 3** is expanded. As mentioned previously, this orbital basis is obtained from partial localization of the natural orbitals in a way that only the $3d_{x^2-y^2}$ and the O 2*p* ZR-like orbitals are localized. Since a large part of electron correlation is compressed in natural orbitals, we see a tiny $s(1)_i$ for all orbitals except for the localized $3d_{x^2-y^2}$ and the O 2*p* ZR-like orbitals where it is significant. This is consistent with the wavefunction in **Table 3**. The mutual orbital entanglement between pairs of orbitals shows strong entanglement between the $3d_{x^2-y^2}$ and the O 2*p* ZR-like orbitals for both $NdNiO_2$ and $CaCuO_2$, a consequence of the dominant weight of the configurations spanned by these two orbitals in the wavefunction. The next strongest entanglement is between the Ni/Cu 3*d* valence and their double-shell 4*d* orbitals. Such strong entanglement also

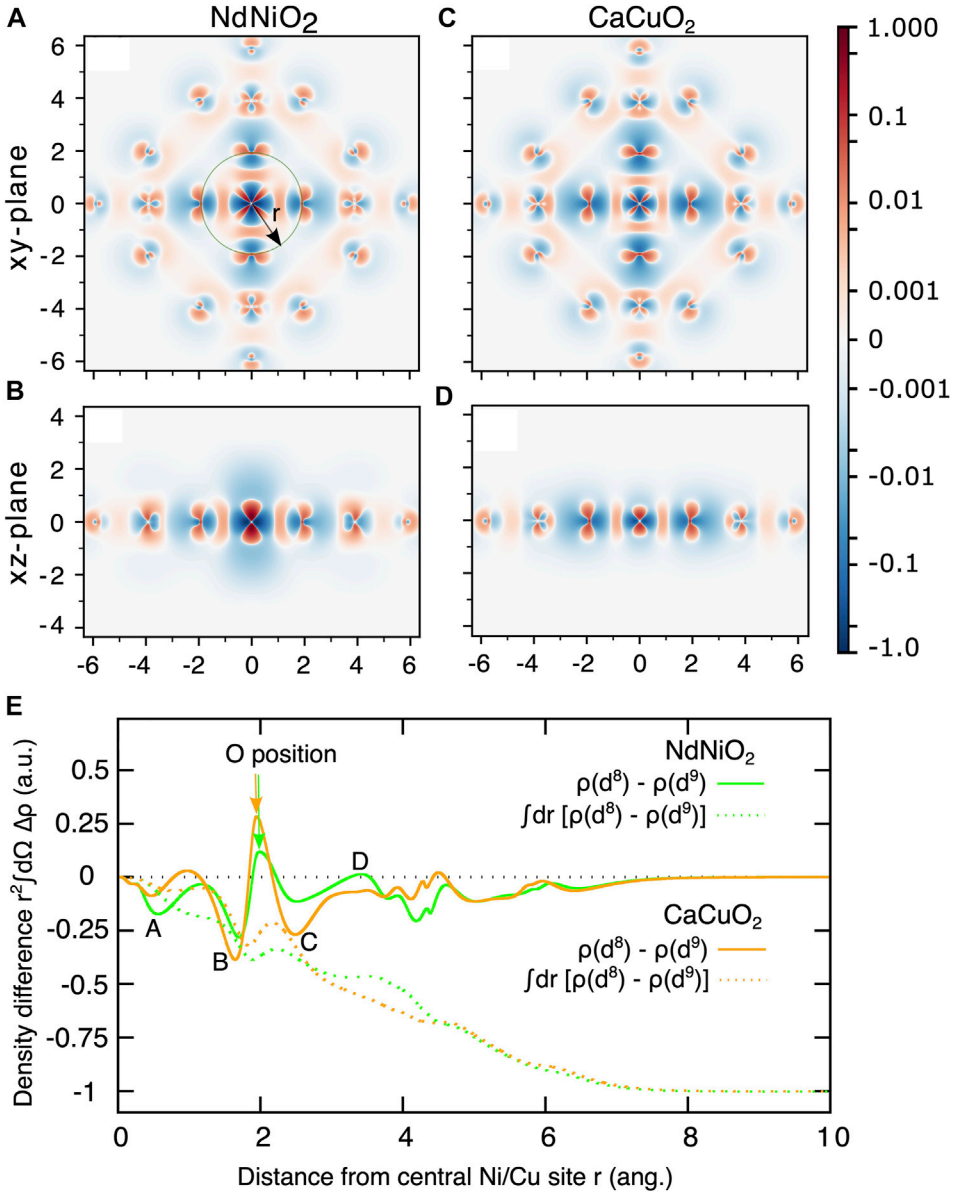

FIGURE 3 | Electron density difference of the d^8 and d^9 ground states ($\rho(d^8)-\rho(d^9)$) for $NdNiO_2$ in the xy-plane **(A)** and xz-plane **(B)**, and for $CaCuO_2$ xy-plane **(C)** and xz-plane **(D)**. The coordinates of the central Ni (Cu) d^8 ion are set to (0,0). The scale of the heat-bar is logarithmic between ±0.001 to ±1.0 and is linear between 0 and ±0.001. **(E)** Electron density difference integrated over a sphere centered on the central Ni(Cu) atoms (full curves) as a function of the radius *r* shown in **(A)**. The result of an additional radial integration (dashed curves) as a function of the upper integration limit.

observed for the undoped d^9 ground state [7], is a result of dynamical radial correlation [18] and orbital breathing effects [63, 64]. Interestingly, the entanglement entropy in the range 0.001–0.01 (green lines) is quite similar in the two compounds, although one sees more entanglement connections in $NdNiO_2$. A comparison of the entropy information between $NdNiO_2$ and $CaCuO_2$ reveals that the Ni 3*d* and 4*d*-like orbitals contribute rather significantly (thicker blue lines) to the total entropy, in contrast to the Cu 3*d* and 4*d*-like orbitals, something that is also seen in the undoped compounds [7].

5 CONCLUSION AND DISCUSSION

In conclusion, our *ab initio* many-body quantum chemistry calculations for the electron removal (d^8) states find a low-spin closed-shell singlet ground state in $NdNiO_2$ and that the additional hole is mainly localized on the Ni $3d_{x^2-y^2}$ orbital, unlike in $CaCuO_2$, where a Zhang-Rice singlet is predominant. We emphasise that the d^8 wavefunction is highly multi-configurational where the dominant closed-shell singlet configuration weight is only ~42%. This result is consistent with the experimental evidence [6, 14] of

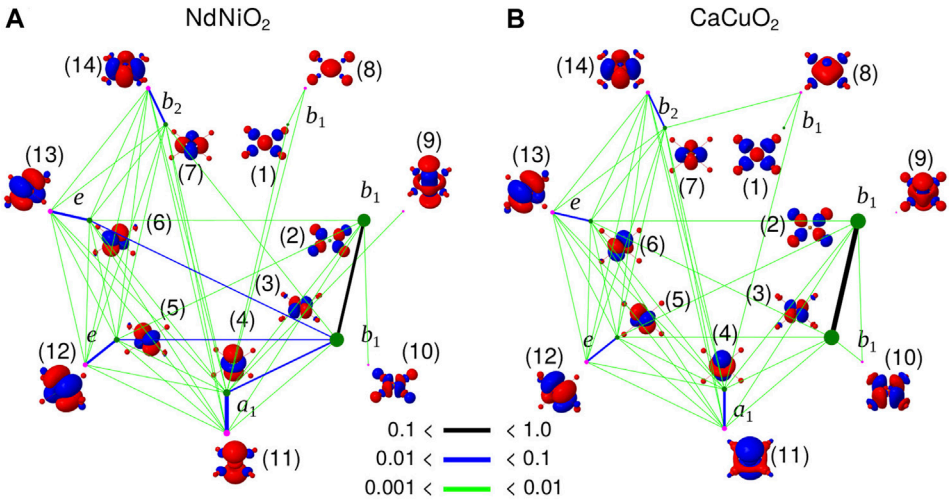

FIGURE 4 | Single orbital entanglement entropy, $s(i)_i$ (dots) and mutual orbital entanglement entropy, $I_{i,j}$ (colored lines) of the orbital basis used to expand the d^8 wavefunction in **Table 3** for $NdNiO_2$ **(A)** and $CaCuO_2$ **(B)**. Entanglement entropy of the orbitals centred on the central NiO_4/CuO_4 plaque are only shown. The irrep to which the orbitals belong to are also shown. The green and magenta colors represent the two different set of orbitals, occupied (at the HF level) and the corresponding double-shell (virtual), respectively. The thickness of the black, blue and green lines denote the strength of $I_{i,j}$, and the size of the dots is proportional to s $(1)_i$. The raw data is presented in **Supplementary Tables S1, S2**.

orbitally polarized singlet state as well as the presence of holes on the O $2p$ orbitals. Importantly, the persistent dynamic radial-type correlations within the Ni d manifold result in stronger d^8 multiplet effects in $NdNiO_2$, and consequently the additional hole foot-print is more three dimensional. In $CaCuO_2$, we find that the electron correlations within the d_{xy} and $d_{xz/yz}$ orbitals changes the hole-doped wavefunction significantly. Specifically, the double hole occupation of Cu $d_{x^2-y^2}$ is significantly increased and this can influence the transport properties.

It was recently proposed that nickelates could be a legitimate realization of the single-band Hubbard model [65]. However, our analysis shows that even the three-band Hubbard model [66], which successfully describes the hole-doped scenario in cuprates, falls short to describe hole-doped nickelates and additional orbital degrees of freedom are indeed necessary for the description of the strong multiplet effects we find. Much has been discussed about the importance of rare-earth atoms for the electronic structure of superconducting nickelates, e.g. see [67]. The three-dimensional nature of the hole density we find in $NdNiO_2$ might also be hinting at the importance of out-of-plane Nd ions. It would be interesting to compare the hole density of $NdNiO_2$ with other iso-structural nickelates such as $LaNiO_2$ where La $5d$ states are far from the Fermi energy. Since the infinite-layered monovalent nickelates are thin films that are grown on substrates, one could ask the question of how the electronic structure of the undoped and doped compounds changes with varying Ni-O bond length. Would this influence the role of electronic correlations in d^9 nickelates? We will address these in the near future.

DATA AVAILABILITY STATEMENT

The data supporting the conclusions of this study can be made available upon reasonable request.

AUTHOR CONTRIBUTIONS

VK and AA designed the project. VK and NB performed the calculations. All the authors analysed the data. VK wrote the paper with inputs from NB and AA.

ACKNOWLEDGMENTS

VK would like to acknowledge Giovanni Li Manni and Oskar Weser for fruitful discussions. We gratefully acknowledge the Max Plank Society for financial support.

SUPPLEMENTARY MATERIAL

The Supplementary Material for this article can be found online at: https://www.frontiersin.org/articles/10.3389/fphy.2022.836784/full#supplementary-material

REFERENCES

1. Bednorz JG, Müller KA. Possible High Tc Superconductivity in the Ba-La-Cu-O System. *Z Physik B - Condensed Matter* (1986) 64:189–93. doi:10.1007/bf01303701
2. Li D, Lee K, Wang BY, Osada M, Crossley S, Lee HR, et al. Superconductivity in an Infinite-Layer Nickelate. *Nature* (2019) 572:624–7. doi:10.1038/s41586-019-1496-5
3. Osada M, Wang BY, Goodge BH, Lee K, Yoon H, Sakuma K, et al. A Superconducting Praseodymium Nickelate with Infinite Layer Structure. *Nano Lett* (2020) 20:5735–40. doi:10.1021/acs.nanolett.0c01392
4. Osada M, Wang BY, Goodge BH, Harvey SP, Lee K, Li D, et al. Nickelate Superconductivity without Rare-Earth Magnetism: (La,Sr)NiO_2. *Adv Mater* (2021) 33:2104083. doi:10.1002/adma.202104083
5. Keimer B, Kivelson SA, Norman MR, Uchida S, Zaanen J. From Quantum Matter to High-Temperature Superconductivity in Copper Oxides. *Nature* (2015) 518:179–86. doi:10.1038/nature14165
6. Rossi M, Lu H, Nag A, Li D, Osada M, Lee K, et al. Orbital and Spin Character of Doped Carriers in Infinite-Layer Nickelates. *Phys. Rev. B* (2021). 104: L220505. doi:10.1103/PhysRevB.104.L220505
7. Katukuri VM, Bogdanov NA, Weser O, van den Brink J, Alavi A. Electronic Correlations and Magnetic Interactions in Infinite-Layer $NdNiO_2$. *Phys Rev B* (2020) 102:241112. doi:10.1103/physrevb.102.241112
8. Moretti Sala M, Bisogni V, Aruta C, Balestrino G, Berger H, Brookes NB, et al. Energy and Symmetry of d-d Excitations in Undoped Layered Cuprates Measured by CuL_3 Resonant Inelastic X-ray Scattering. *New J Phys* (2011) 13:043026. doi:10.1088/1367-2630/13/4/043026
9. Lee K-W, Pickett WE. Infinite-Layer $LaNiO_2$: Ni^{1+} is not Cu^{2+}. *Phys Rev B* (2004) 70:165109. doi:10.1103/physrevb.70.165109
10. Liu Z, Ren Z, Zhu W, Wang Z, Yang J. Electronic and Magnetic Structure of Infinite-Layer $NdNiO_2$: Trace of Antiferromagnetic Metal. *Npj Quan Mater* (2020) 5:31. doi:10.1038/s41535-020-0229-1
11. Zhang H, Jin L, Wang S, Xi B, Shi X, Ye F, et al. Effective Hamiltonian for Nickelate Oxides $Nd_{1-x}Sr_xNiO_2$. *Phys Rev Res* (2020) 2:013214. doi:10.1103/physrevresearch.2.013214
12. Zaanen J, Sawatzky GA, Allen JW. Band Gaps and Electronic Structure of Transition-Metal Compounds. *Phys Rev Lett* (1985) 55:418–21. doi:10.1103/physrevlett.55.418
13. Hepting M, Li D, Jia CJ, Lu H, Paris E, Tseng Y, et al. Electronic Structure of the Parent Compound of Superconducting Infinite-Layer Nickelates. *Nat Mater* (2020) 19:381–5. doi:10.1038/s41563-019-0585-z
14. Goodge BH, Li D, Lee K, Osada M, Wang BY, Sawatzky GA, et al. Doping Evolution of the Mott–Hubbard Landscape in Infinite-Layer Nickelates. *Proc Natl Acad Sci* (2021) 118:e2007683118. doi:10.1073/pnas.2007683118
15. Zhang FC, Rice TM. Effective Hamiltonian for the Superconducting Cu Oxides. *Phys Rev B* (1988) 37:3759–61. doi:10.1103/physrevb.37.3759
16. Jiang M, Berciu M, Sawatzky GA. Critical Nature of the Ni Spin State in Doped $NdNiO_2$. *Phys Rev Lett* (2020) 124:207004. doi:10.1103/physrevlett.124.207004
17. Plienbumrung T, Schmid MT, Daghofer M, Oleś AM. Character of Doped Holes in $Nd_{1-x}Sr_xNiO_2$. *Condensed Matter* (2021) 6:33. doi:10.3390/condmat6030033
18. Helgaker T, Jørgensen P, Olsen J. *Molecular Electronic-Structure Theory*. Chichester: Wiley (2000).
19. Muñoz D, Illas F, de P. R. Moreira I. Accurate Prediction of Large Antiferromagnetic Interactions in High-Tc $HgBa_2Ca_{\{n-1\}}Cu_nO_{\{2n+2+\}}$ (n=2,3) Superconductor Parent Compounds. *Phys Rev Lett* (2000) 84: 1579–82. doi:10.1103/physrevlett.84.1579
20. Hozoi L, Siurakshina L, Fulde P, van den Brink J. Ab Initio determination of Cu 3d Orbital Energies in Layered Copper Oxides. *Sci Rep* (2011) 1:65. doi:10.1038/srep00065
21. Hozoi L, Fulde P. *Computational Methods for Large Systems: Electronic Structre Approaches for Biotechnology and Nanotechnology*. Hoboken: John Wiley & Sons (2011). Chap. 6.
22. Bogdanov NA, van den Brink J, Hozoi L. Ab Initio Computation of d-d Excitation Energies in Low-Dimensional Ti and V Oxychlorides. *Phys Rev B* (2011) 84:235146. doi:10.1103/physrevb.84.235146
23. Katukuri VM, Stoll H, van den Brink J, Hozoi L. Ab Initio Determination of Excitation Energies and Magnetic Couplings in Correlated Quasi-Two-Dimensional Iridates. *Phys Rev B* (2012) 85:220402. doi:10.1103/physrevb.85.220402
24. Bogdanov NA, Maurice R, Rousochatzakis I, van den Brink J, Hozoi L. Magnetic State of Pyrochlore $Cd_2Os_2O_7$ Emerging from Strong Competition of Ligand Distortions and Longer-Range Crystalline Anisotropy. *Phys Rev Lett* (2013) 110:127206. doi:10.1103/physrevlett.110.127206
25. Gretarsson H, Clancy JP, Liu X, Hill JP, Bozin E, Singh Y, et al. Crystal-field Splitting and Correlation Effect on the Electronic Structure of A_2IrO_3. *Phys Rev Lett* (2013) 110:076402. doi:10.1103/PhysRevLett.110.076402
26. Katukuri VM, Yushankhai V, Siurakshina L, Brink JVD, Hozoi L, Rousochatzakis I. Mechanism of Basal-Plane Antiferromagnetism in the Spin-Orbit Driven Iridate Ba_2IrO_4. *Phys Rev X* (2014) 4:021051. doi:10.1103/physrevx.4.021051
27. Katukuri VM, Nishimoto S, Yushankhai V, Stoyanova A, Kandpal H, Choi S, et al. Kitaev Interactions Between j= 1/2 Moments in Honeycomb Na_2IrO_3 are Large and Ferromagnetic: Insights From Ab Initio Quantum Chemistry Calculations. *New J Phys* (2014) 16:013056. doi:10.1088/1367-2630/16/1/013056
28. Fulde P. *Correlated Electrons in Quantum Matter*. Singapore: World Scientific (2012).
29. Klintenberg M, Derenzo SE, Weber MJ. Accurate crystal fields for Embedded Cluster Calculations. *Comput Phys Commun* (2000) 131:120–8. doi:10.1016/s0010-4655(00)00071-0
30. Katukuri VM, Roszeitis K, Yushankhai V, Mitrushchenkov A, Stoll H, van Veenendaal M, et al. Electronic Structure of Low-Dimensional $4d^5$ Oxides: Interplay of Ligand Distortions, Overall Lattice Anisotropy, and Spin-Orbit Interactions. *Inorg Chem* (2014) 53:4833–9. doi:10.1021/ic402653f
31. Babkevich P, Katukuri VM, Fåk B, Rols S, Fennell T, Pajić D, et al. Magnetic Excitations and Electronic Interactions in Sr_2CuTeO_6: A Spin-1/2 Square Lattice Heisenberg Antiferromagnet. *Phys Rev Lett* (2016) 117:237203. doi:10.1103/physrevlett.117.237203
32. Booth GH, Thom AJW, Alavi A. Fermion Monte Carlo without Fixed Nodes: a Game of Life, Death, and Annihilation in Slater Determinant Space. *J Chem Phys* (2009) 131:054106. doi:10.1063/1.3193710
33. Cleland D, Booth GH, Alavi A. Communications: Survival of the Fittest: Accelerating Convergence in Full Configuration-Interaction Quantum Monte Carlo. *J Chem Phys* (2010) 132:041103. doi:10.1063/1.3302277
34. Guther K, Anderson RJ, Blunt NS, Bogdanov NA, Cleland D, Dattani N, et al. NECI: N-Electron Configuration Interaction with an Emphasis on State-Of-The-Art Stochastic Methods. *J Chem Phys* (2020) 153:034107. doi:10.1063/5.0005754
35. Chan GK-L, Sharma S. The Density Matrix Renormalization Group in Quantum Chemistry. *Annu Rev Phys Chem* (2011) 62:465–81. doi:10.1146/annurev-physchem-032210-103338
36. Sharma S, Chan GK-L. Spin-adapted Density Matrix Renormalization Group Algorithms for Quantum Chemistry. *J Chem Phys* (2012) 136:124121. doi:10.1063/1.3695642
37. Andersson K, Malmqvist PÅ, Roos BO. Second-order Perturbation Theory with a Complete Active Space Self-consistent Field Reference Function. *J Chem Phys* (1992) 96:1218–26. doi:10.1063/1.462209
38. Angeli C, Cimiraglia R, Evangelisti S, Leininger T, Malrieu J-P. Introduction Of N-Electron Valence States for Multireference Perturbation Theory. *J Chem Phys* (2001) 114:10252–64. doi:10.1063/1.1361246
39. Emery VJ. Theory of High-Tc superconductivity in Oxides. *Phys Rev Lett* (1987) 58:2794–7. doi:10.1103/physrevlett.58.2794
40. Jiang M, Moeller M, Berciu M, Sawatzky GA. Relevance of Cu-3d Multiplet Structure in Models of High-T_c Cuprates. *Phys Rev B* (2020) 101:035151. doi:10.1103/physrevb.101.035151
41. Plienbumrung T, Daghofer M, Oleś AM. Interplay between Zhang-Rice Singlets and High-Spin States in a Model for Doped NiO_2 Planes. *Phys Rev B* (2021) 103:104513. doi:10.1103/physrevb.103.104513

42. Hayward MA, Rosseinsky MJ. Synthesis of the Infinite Layer Ni(I) Phase $NdNiO_{2+x}$ by Low Temperature Reduction of $NdNiO_3$ with Sodium Hydride. *Solid State Sci* (2003) 5:839–50. doi:10.1016/s1293-2558(03)00111-0
43. Kobayashi N, Hiroi Z, Takano M. Compounds and Phase Relations in the SrO-CaO-CuO System under High Pressure. *J Solid State Chem* (1997) 132:274–83. doi:10.1006/jssc.1997.7442
44. Karpinski J, Mangelschots I, Schwer H, Conder K, Morawski A, Lada T, et al. Single crystal Growth of HgBaCaCuO and Infinite Layer $CaCuO_2$ at High Gas Pressure. *Physica C: Superconductivity* (1994) 235-240:917–8. doi:10.1016/0921-4534(94)91683-7
45. Dolg M, Wedig U, Stoll H, Preuss H. Energy-adjusted ab Initio Pseudopotentials for the First Row Transition Elements. *J Chem Phys* (1987) 86:866–72. doi:10.1063/1.452288
46. Martin JML, Sundermann A. Correlation Consistent Valence Basis Sets for Use with the Stuttgart-Dresden-Bonn Relativistic Effective Core Potentials: The Atoms Ga-Kr and In-Xe. *J Chem Phys* (2001) 114:3408–20. doi:10.1063/1.1337864
47. Roos BO, Lindh R, Malmqvist P-Å, Veryazov V, Widmark P-O. Main Group Atoms and Dimers Studied with a New Relativistic ANO Basis Set. *J Phys Chem A* (2004) 108:2851–8. doi:10.1021/jp031064+
48. Dolg M, Stoll H, Savin A, Preuss H. Energy-adjusted Pseudopotentials for the Rare Earth Elements. *Theoret Chim Acta* (1989) 75:173–94. doi:10.1007/bf00528565
49. Dolg M, Stoll H, Preuss H. A Combination of Quasirelativistic Pseudopotential and Ligand Field Calculations for Lanthanoid Compounds. *Theoret Chim Acta* (1993) 85:441–50. doi:10.1007/bf01112983
50. Kaupp M, Schleyer Pv. R, Stoll H, Preuss H. Pseudopotential Approaches to Ca, Sr, and Ba Hydrides. Why Are Some Alkaline Earth MX_2 Compounds Bent? *J Chem Phys* (1991) 94:1360–6. doi:10.1063/1.459993
51. Igel-Mann G. Ph.D. thesis. Stuttgart: University of Stuttgart (1987). Untersuchungen an Hauptgruppenelementen und Nebengruppenelementen mit abgeschlossener d-Schale
52. University of Cologne. Energy-consistent Pseudopotentials of Stuttgart/Cologne Group (2014). Available at: http://www.tc.uni-koeln.de/cgi-bin/pp.pl?language=en,format=molpro,element=Zn,job=getecp,ecp=ECP28SDF (Accessed Sept 15, 2021).
53. Fdez. Galván I, Vacher M, Alavi A, Angeli C, Aquilante F, Autschbach J, et al. OpenMolcas: From Source Code to Insight. *J Chem Theor Comput.* (2019) 15:5925–64. doi:10.1021/acs.jctc.9b00532
54. Jmol. *Jmol: An Open-source Java Viewer for Chemical Structures in 3D* (2001). Available from: http://www.jmol.org/.
55.. For an accurate quantitative description of the multiplet structure spanned by the other two irreps b_1 and e, one would need to extend the active space and include the 3d and 4d manifolds of the four neighbouring Ni (Cu) atoms as well as the O 2p orbitals of the same symmetry, resulting in a gigantic 68 electrons in 74 orbitals active space.
56. Lu T, Chen F. Multiwfn: A Multifunctional Wavefunction Analyzer. *J Comput Chem* (2012) 33:580–92. doi:10.1002/jcc.22885
57. Boguslawski K, Tecmer P, Legeza Ö, Reiher M. Entanglement Measures for Single- and Multireference Correlation Effects. *J Phys Chem Lett* (2012) 3:3129–35. doi:10.1021/jz301319v
58. Boguslawski K, Tecmer P, Barcza G, Legeza Ö, Reiher M. Orbital Entanglement in Bond-Formation Processes. *J Chem Theor Comput.* (2013) 9:2959–73. doi:10.1021/ct400247p
59. Boguslawski K, Tecmer P. Orbital Entanglement in Quantum Chemistry. *Int J Quan Chem.* (2015) 115:1289–95. doi:10.1002/qua.24832
60. Legeza Ö, Sólyom J. Optimizing the Density-Matrix Renormalization Group Method Using Quantum Information Entropy. *Phys Rev B* (2003) 68:195116. doi:10.1103/physrevb.68.195116
61. Rissler J, Noack RM, White SR. Measuring Orbital Interaction Using Quantum Information Theory. *Chem Phys* (2006) 323:519–31. doi:10.1016/j.chemphys.2005.10.018
62. Keller S, Dolfi M, Troyer M, Reiher M. An Efficient Matrix Product Operator Representation of the Quantum Chemical Hamiltonian. *J Chem Phys* (2015) 143:244118. doi:10.1063/1.4939000
63. Gunnarsson O, Andersen OK, Jepsen O, Zaanen J. Density-functional Calculation of the Parameters in the Anderson Model: Application to Mn in CdTe. *Phys Rev B* (1989) 39:1708–22. doi:10.1103/physrevb.39.1708
64. Bogdanov NA, Li Manni G, Sharma S, Gunnarsson O, Alavi A. Enhancement of Superexchange Due to Synergetic Breathing and Hopping in Corner-Sharing Cuprates. *Nat Phys* (2021) 18:190–5. doi:10.1038/s41567-021-01439-1
65. Kitatani M, Si L, Janson O, Arita R, Zhong Z, Held K. Nickelate Superconductors – a Renaissance of the One-Band Hubbard Model. *npj Quan Mater* (2020) 5:59. doi:10.1038/s41535-020-00260-y
66. Eskes H, Sawatzky GA. Single-, Triple-, or Multiple-Band Hubbard Models. *Phys Rev B* (1991) 44:9656–66. doi:10.1103/physrevb.44.9656
67. Nomura Y, Arita R. Superconductivty in Infinite-Layer Nickelates. *Rep. Prog. Phys.* (2021) 85:052501. doi:10.1088/1361-6633/ac5a60

Conflict of Interest: The authors declare that the research was conducted in the absence of any commercial or financial relationships that could be construed as a potential conflict of interest.

Publisher's Note: All claims expressed in this article are solely those of the authors and do not necessarily represent those of their affiliated organizations, or those of the publisher, the editors, and the reviewers. Any product that may be evaluated in this article, or claim that may be made by its manufacturer, is not guaranteed or endorsed by the publisher.